

Phase-Noise Analysis of Optically Generated Millimeter-Wave Signals With External Optical Modulation Techniques

Guohua Qi, Jianping Yao, *Senior Member, IEEE*, Joe Seregelyi, Stéphane Paquet, Claude Bélisle, Xiupu Zhang, *Member, IEEE*, Ke Wu, *Fellow, IEEE*, and Raman Kashyap

Abstract—In this paper, the phase-noise performance of optically generated electrical signals based on external optical modulation techniques is investigated theoretically and experimentally. Mathematical models are developed to represent perturbations on the transmitted optical signal caused by the phase fluctuations of the electrical drive signal applied to the external modulator and the optical carrier that feeds the external modulator. Closed-form expressions of the power spectral density (PSD) for the electrical signals, generated both locally and remotely, are derived. The calculated PSD of the locally generated electrical signal indicates that its phase noise is determined only by the phase noise of the electrical drive signal. The PSD of the remotely generated signal shows that its spectral quality is also affected by the chromatic dispersion of the fiber and the optical carrier linewidth. An experimental setup that can generate a millimeter-wave (mm-wave) signal, continuously tunable from 32 to 60 GHz using an electrical drive signal tunable from 8 to 15 GHz, is built. The spectra of the generated millimeter-wave signal are measured for both locally and remotely generated electrical signals, with optical carriers of different linewidths. The theoretical results agree with the experimental measurements.

Index Terms—Microwave photonics, millimeter-wave (mm-wave) generation, optical fiber dispersion, optical modulation, phase noise, radio over fiber, spectral analysis.

I. INTRODUCTION

OPTICAL LINKS have been widely used for the transmission of high-speed digital baseband signals because of the inherent low loss, low dispersion, and wide bandwidth of single-mode fibers, combined with the possibility of using optical amplifiers to compensate for the loss [1]. For similar reasons, the use of optical links in wireless communication systems has increasingly attracted attention [2]–[5]. The advantages of optical links are even more noticeable when delivering radio frequency (RF), microwave, or millimeter-wave (mm-wave) signals over long distances, for example, between a

Manuscript received November 9, 2005; revised August 28, 2006. This work was supported in part by the Canadian Institute for Photonic Innovations and The Natural Sciences and Engineering Research Council of Canada.

G. Qi and J. Yao are with the Microwave Photonics Research Laboratory, School of Information Technology and Engineering, University of Ottawa, Ottawa, ON K1N 6N5, Canada (e-mail: jpyao@site.uottawa.ca).

J. Seregelyi, S. Paquet, and C. Bélisle are with the Communications Research Centre Canada, Ottawa, ON K2H 8S2, Canada.

X. Zhang is with the Department of Electrical and Computer Engineering, Concordia University, Montreal, QC H3G 1M8, Canada.

K. Wu and R. Kashyap are with the Ecole Polytechnique de Montreal, Montreal, QC H3C 3A7, Canada.

Digital Object Identifier 10.1109/JLT.2006.884990

central office and base stations. They are particularly useful in applications like broadband wireless access networks [6], [7], and they have also found applications in military systems, such as antenna remoting, Doppler radar, and phased array antennas [8]–[10].

Key to this technology is the generation and distribution of microwave or millimeter-wave signals in the optical domain. In the past, extensive investigations of optical microwave generation systems have led to a variety of electrical-signal-generation methods. These methods employ techniques such as automatic frequency control loop [11], optical injection locking [12], optical phase-locked loop (OPLL) [13], [14], and external modulation [15]–[20]. The short- and long-term frequency stability of the optically generated millimeter-wave signals is critical because the resulting signal is generally used either as an RF carrier or a local oscillator signal in system applications. Optical frequency locking, optical injection locking, and OPLL have all been used to improve the long-term frequency stability. An OPLL, when used in conjunction with a narrow linewidth optical source, can generate a millimeter-wave signal with high short-term frequency stability [21]. The short-term stability is directly related to the spectral purity of the generated signal, and it can be characterized with phase-noise measurement techniques.

Among the aforementioned signal-generation methods, those using external-modulation techniques have shown great potential for producing high-purity and frequency tunable microwave or millimeter-wave signals [15], [19]. Owing to the inherent nonlinearity of the external modulator, microwave generation techniques using external modulation enable the generation of microwave or millimeter-wave signals with a frequency that is two or four times that of the electrical drive signal, which makes the use of low-frequency low-cost external modulator possible. In 1994, O'Reilly applied such a method for the remote delivery of video services [22].

External-modulation-based signal-generation schemes are built using a laser source, an electrical microwave source, an optical intensity or phase modulator, a photodetector, and/or an optical filter. The microwave signals can be generated locally prior to fiber propagation and remotely after having propagated in a given length of optical fiber. For many applications, it is important to explore the quality of the generated electrical signal, especially its noise characteristics.

A number of previously published papers [23]–[29] have covered the modeling and measurement of signal phase noise

in optical links within various contexts. For instance, a phase noise caused by multiple reflections in an externally modulated optical link has been analyzed in [23]. A technique for measuring residual single sideband (SSB) microwave phase noise, added by an externally modulated fiber-optic link, was reported in [24]. A model for calculating additive phase noise in direct-modulation optical links was presented in [25]. Chromatic-dispersion effects on the phase noise of optical millimeter-wave systems were investigated in [26] and [27] for direct and remote heterodyne detection. Effects of the amplified spontaneous emission (ASE) noise of an erbium-doped fiber amplifiers (EDFA) on the spectral broadening of optically generated electrical signals were experimentally examined in [28] and [29]. However, no reports have covered the modeling of the phase noise in an external modulator-based generation system by considering the phase noise of the electrical drive signal.

In this paper, we present a theoretical and experimental investigation of the phase noise of an optically generated electrical signal by the external optical modulation technique. As part of this analysis, closed-form expressions for the power spectral density (PSD) of the locally and remotely generated electrical signal are derived. An experimental setup is built to validate the theoretical analysis. The experimental setup can generate a continuously tunable millimeter-wave signal from 32 to 60 GHz with the electrical drive signal tuned from 8 to 15 GHz. The experimental measurements have verified that the phase noise of the locally generated millimeter-wave signal is independent of the effect of active optical components used in the system. In effect, the phase-noise deterioration of the locally generated millimeter-wave signal can be modeled using the same theory employed for electronic frequency multipliers. Experimental results also showed that the phase noise of a remotely generated millimeter-wave signal has no noticeable phase-noise deterioration compared with the locally generated electrical signal for transmission distances of 25 and 50 km over a standard single-mode fiber (SSMF). These results are valid for optical sources with spectral widths of 700 kHz and 50 MHz. All these experimental results agree well with the theoretical PSD analysis. However, based on our theoretical analysis, using a low-coherence optical source or extending the transmission length of the fiber will bring noticeable phase-noise deterioration to the remotely generated millimeter-wave signal since the phase correlation between the optical sidebands is reduced. A sliced ASE source as an optical carrier with a 3-dB linewidth of 33 GHz is examined for different transmission distances over SSMF.

This paper is organized as follows. In Section II, mathematical models representing the generation of local and remote electrical signal using an external modulator are presented. Then, phase-noise analysis of the electrical drive signal using the PSD of its phase fluctuation is performed in Section III. A review of the circuit-theory representation of phase noise as a fractional power series of frequency is also presented in this section. Phase noise of the locally generated electrical signal is analyzed in Section IV. Phase noise of the remotely generated electrical signal is analyzed in Section V. Experimental results and the validation of the theoretical models are detailed in Section VI. Last, conclusions are given in Section VII.

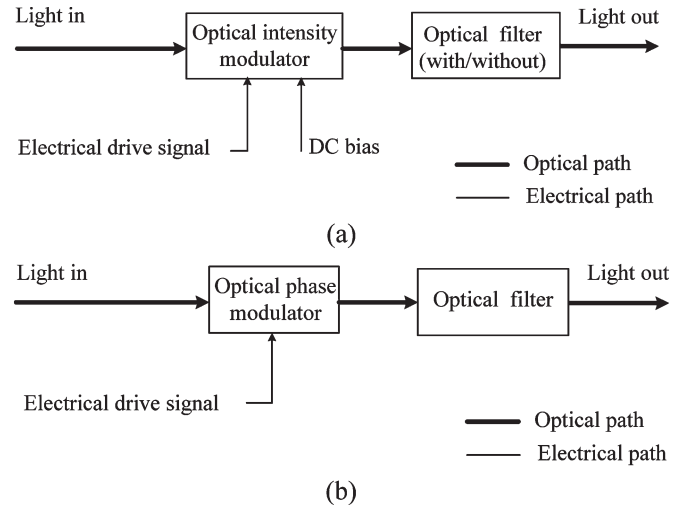


Fig. 1. Diagrams of systems for electrical signal generation based on external optical modulation techniques. (a) Optical intensity modulator-based system. (b) Optical phase modulator-based system.

II. OPTICAL MICROWAVE GENERATION BASED ON EXTERNAL OPTICAL MODULATION TECHNIQUES

Systems used for generating millimeter-wave signals based on external-modulation techniques [15]–[20] can be generally classified into two types: phase modulator and intensity modulator-based configurations. They are shown in Fig. 1.

The configuration using an intensity modulator can be designed with or without an optical filter. For example, the studies in [15] and [19] presented a design that did not use an optical filter. A design that includes an optical filter was demonstrated in [16]. By properly biasing the intensity modulator, the odd-order sidebands were suppressed. The optical carrier was then removed with the inclusion of a narrowband optical notch filter. A fourth-order harmonic of the electrical drive signal was thus generated. In the configuration using a phase modulator, the creation of the electrical signal requires the use of an optical filter [17], [20]. This is because the beating between the optical carrier and the optical sidebands at a photodetector will cancel completely the harmonics, and only a dc component is generated at the photodetector. This is understandable because the phase modulation will not alter the amplitude of the modulated optical signal and a photodetector acts as an envelope detector. The use of an optical filter after the phase modulator to remove the optical carrier will lead to the generation of second- and fourth-order harmonics. The studies in [18] and [20] discuss various filtering configurations, such as cascading the optical phase modulator with an optical polarizer, incorporating the optical phase modulator in an optical loop mirror or a Faraday mirror, or the use of a narrowband fiber Bragg grating (FBG) notch filter. In the remainder of this paper, we will use the configuration shown Fig. 1 for our theoretical analysis and experimental verifications.

Both the electrical signal and optical signal in Fig. 1 have a finite spectral width due to the phase fluctuations of the signal. Phase fluctuations for a single-frequency laser can be caused by, for example, a refractive index variation in the laser due to temperature changes and carrier concentration effects.

For the electrical source, the phase fluctuation comes from the thermal noise, the shot noise, and the $1/f$ noise [30]. All these phase fluctuations bear random characteristics. The phase-noise statistics of the optical carrier and the electrical drive source are treated as two independent random processes, which will define the spectral quality of the generated electrical signal. Phase fluctuations of a signal can be interpreted as a parasitic phase modulation of an ideal sinusoidal signal [30], [31]. This interpretation is valid for both the electrical drive signal and optical carrier in Fig. 1. It is assumed that both the optical carrier and the electrical drive signal are continuous wave (CW) in nature. Therefore, they can be expressed as

$$E(t) = E_o \cos [\omega_o t + \phi_o(t)] \quad (1)$$

and

$$V(t) = V_e \cos [\omega_e t + \phi_e(t)] \quad (2)$$

where $E(t)$ is the electric field of the optical carrier in scalar form (scalar form is used based on the assumption that the light is linearly polarized and it is aligned with the corresponding polarization state axis of the modulator), and $V(t)$ is the voltage of the electrical drive signal. E_o and ω_o are the electric field amplitude and angular frequency ($\omega_o = 2\pi f_o$) of the optical carrier. V_e and ω_e are the voltage amplitude and angular frequency ($\omega_e = 2\pi f_e$) of the electrical drive signal. Finally, $\phi_o(t)$ and $\phi_e(t)$ are two independent random processes that introduce phase fluctuations to the optical and electrical signals, respectively. It must be emphasized that we are studying a case where the phase noise is dominant and amplitude or intensity noise can be neglected due to the presence of limiting mechanisms in the electrical and optical source. It is true for most quality electrical and optical sources. Thus, E_o and V_e are assumed to be constant. For many fiber links, amplitude-modulation (AM) noise of the link can be dominant and even exceed the phase-noise contribution of the link, especially after many stages of optical amplification, but in an optical source, not a link, the link noise is much smaller than the phase noise of the source. Many experimental reports have verified that there is no obvious spectral broadening observed due to the link AM noise [28], [29].

A. Optical Microwave Generation Based on an Optical Intensity Modulator

The optical signal at the output of an intensity modulator, which is shown in Fig. 1(a), is given by [32]

$$E_1(t) = E_o \cos \left\{ \frac{\phi_{\text{DC}}}{2} + \beta_i \cos [\omega_e t + \phi_e(t)] \right\} \cdot \cos [\omega_o t + \phi_o(t)] \quad (3)$$

where ϕ_{DC} is the constant phase shift determined by the dc bias voltage, and β_i is a modulation index expressed as

$$\beta_i = \frac{\pi}{V_{\pi_i}} \cdot \frac{V_e}{2} \quad (4)$$

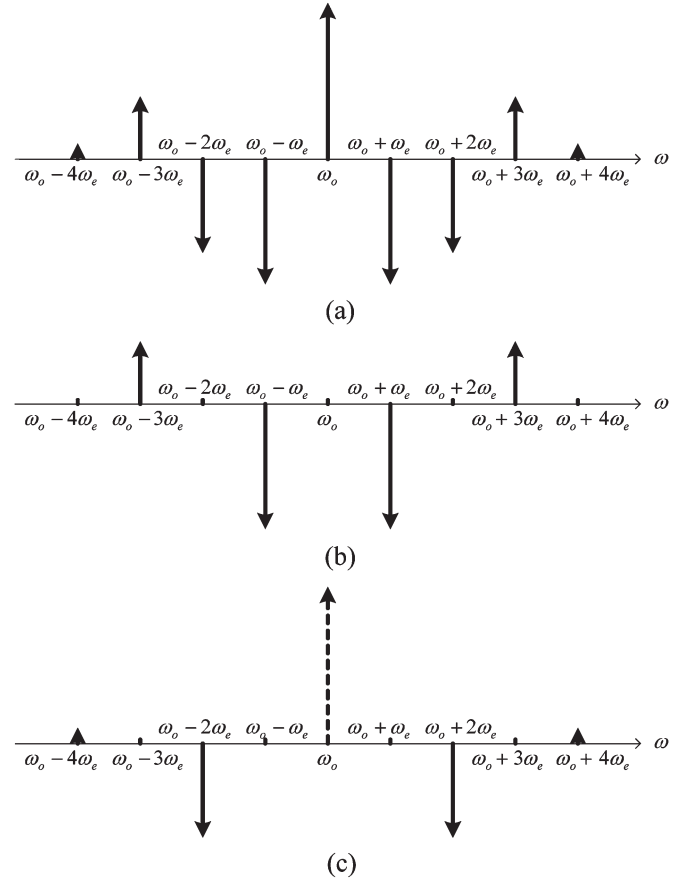


Fig. 2. Typical optical spectra generated by an optical intensity modulator. The arrow direction shows the relationship between the phase of the sidebands and the phase of the optical carrier. (a) A general spectrum. (b) Even-order optical sidebands suppressed. (c) Odd-order optical sidebands and the optical carrier suppressed.

where V_{π_i} is the half-wave voltage of the intensity modulator. Expanding (3), we have

$$\begin{aligned} E_1(t) = & E_o \cos \left(\frac{\phi_{\text{DC}}}{2} \right) J_0(\beta_i) \cos [\omega_o t + \phi_o(t)] \\ & + E_o \cos \left(\frac{\phi_{\text{DC}}}{2} \right) \sum_{n=1}^{\infty} J_{2n}(\beta_i) \\ & \times \{ \cos [\omega_o t - 2n\omega_e t + \phi_o(t) - 2n\phi_e(t) + n\pi] \\ & \quad + \cos [\omega_o t + 2n\omega_e t + \phi_o(t) + 2n\phi_e(t) - n\pi] \} \\ & + E_o \sin \left(\frac{\phi_{\text{DC}}}{2} \right) \sum_{n=1}^{\infty} J_{2n-1}(\beta_i) \\ & \times \{ \cos [\omega_o t - (2n-1)\omega_e t + \phi_o(t) - (2n-1)\phi_e(t) + n\pi] \\ & \quad + \cos [\omega_o t + (2n-1)\omega_e t + \phi_o(t) \\ & \quad \quad + (2n-1)\phi_e(t) - n\pi] \} \end{aligned} \quad (5)$$

where J_n is the Bessel function of the first kind of order n . Equation (5) shows that the power of the input optical carrier spreads to the first-, second-, third-, and higher order optical sidebands. The amplitude of these sidebands is governed by the corresponding order of Bessel function parameterized by β_i . Their amplitude is also affected by ϕ_{DC} . Fig. 2(a) shows a general optical spectrum obtained from (5).

Different values of ϕ_{DC} can be obtained by adjusting the dc bias. There are two sets of important values: $\phi_{DC} = 2k\pi$ and $\phi_{DC} = (2k - 1)\pi$, where k is an integer. When $\phi_{DC} = (2k - 1)\pi$, all even-order optical sidebands disappear. Fig. 2(b) shows the optical spectrum when even-order optical sidebands are suppressed by tuning the dc bias. With an appropriate power level of the electrical drive signal, the second- and higher order optical sidebands can be ignored. The beating between the two first-order sidebands will lead to the generation of a microwave signal that has two times the frequency of the electrical drive signal. An optical filter is not required for this configuration [15]. In this specific scenario, (5) is reduced to

$$E_{I1}(t) = -E_o J_1(\beta_i) \{ \cos [(\omega_o - \omega_e)t + \phi_o(t) - \phi_e(t)] + \cos [(\omega_o + \omega_e)t + \phi_o(t) + \phi_e(t)] \}. \quad (6)$$

O'Reilly and Lane [16] proposed another approach by biasing the intensity modulator to meet the $\phi_{DC} = 2k\pi$ condition, which can be used to generate an electrical signal having four times the frequency of the electrical drive signal. In their system, they used an unbalanced Mach-Zehnder interferometer with a specific free spectral range to select the second-order optical sidebands, and, therefore improve the suppression of the unwanted optical sidebands. In this approach, the optical intensity modulator is biased at 0 V. In the experimental section of this paper, we will demonstrate a simplified approach to generating a microwave frequency that has four times the frequency of the electrical drive signal. A key device in our approach is a narrowband FBG notch filter. The optical intensity modulator is biased to have a constant optical phase of $\phi_{DC} = 2k\pi$ to suppress the odd-order optical sidebands. The optical notch filter is placed at the output of the optical intensity modulator to filter out the optical carrier (the zero order in (5)). Fig. 2(c) shows the optical spectrum when the odd-order optical sidebands are suppressed and the optical carrier (the dashed line) is removed. Using an appropriate power level for the electrical drive signal, optical sidebands of orders higher than the second have very low power and can be ignored. Then, an optical microwave generation system having a similar optical spectrum as in [16] is obtained. Since we use a fixed FBG notch filter, the frequency separation of the two optical sidebands in our approach can be continuously tuned by changing the frequency of the electrical drive signal. Therefore, a continuously frequency tunable millimeter-wave signal can be generated. In our configuration and the one described in [16], (5) is reduced to

$$E_{I2}(t) = E_o J_2(\beta_i) \{ \cos [(\omega_o - 2\omega_e)t + \phi_o(t) - 2\phi_e(t)] + \cos [(\omega_o + 2\omega_e)t + \phi_o(t) + 2\phi_e(t)] \}. \quad (7)$$

B. Optical Microwave Generation Based on an External Optical Phase Modulator

When the optical carrier and electrical drive signal in (1) and (2) are applied to an optical phase modulator [case shown in

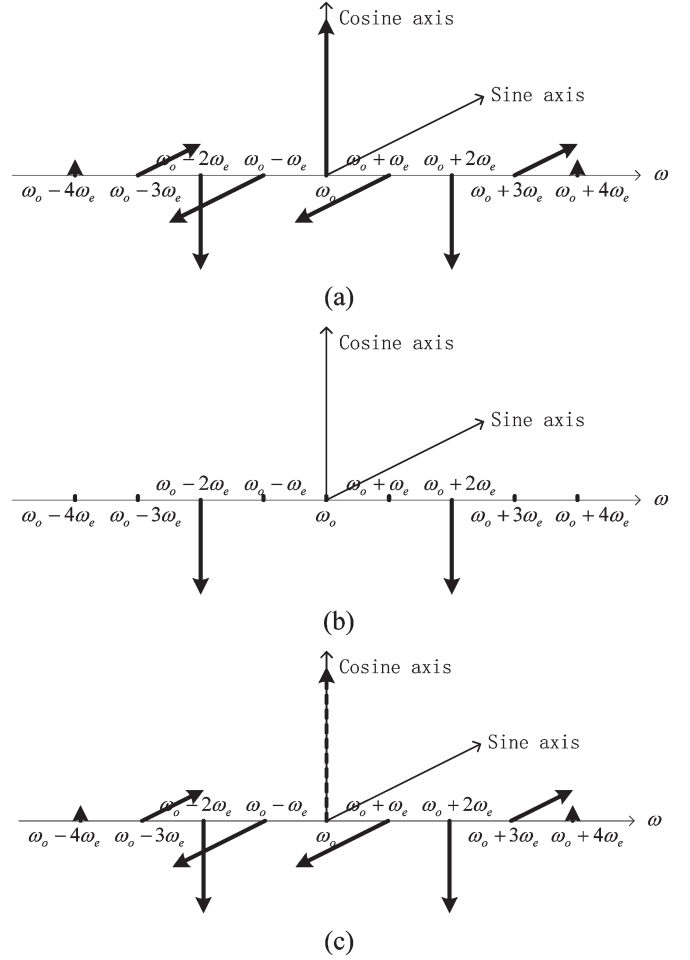


Fig. 3. Typical optical spectra generated by an optical phase modulator. (a) A general spectrum. (b) Filtered spectrum with an F-P filter. (c) Filtered spectrum with an FBG notch filter.

Fig. 1(b)], the optical field at its output is given by

$$\begin{aligned} E_P(t) &= E_o \cos [\omega_o t + \phi_o(t) + \beta_p \cos [\omega_e t + \phi_e(t)]] \\ &= E_o \sum_{n=-\infty}^{+\infty} J_n(\beta_p) \\ &\quad \times \cos \left[(\omega_o + n\omega_e)t + \phi_o(t) + n\phi_e(t) + n\frac{\pi}{2} \right] \quad (8) \end{aligned}$$

where $\beta_p = (\pi/V_{\pi p}) \cdot V_e$, $V_{\pi p}$ is the half-wave voltage of the optical phase modulator. J_n is defined as before. A typical spectrum calculated from (8) is shown in Fig. 3(a).

Various configurations have been suggested using a phase modulator. The approach in [17] used a Fabry-Pérot filter to select the second-order optical sidebands at the output of the phase modulator. The corresponding optical spectrum is shown in Fig. 3(b). For this configuration, (8) is reduced to

$$E_{P1}(t) = -E_o J_2(\beta_p) \{ \cos [(\omega_o - 2\omega_e)t + \phi_o(t) - 2\phi_e(t)] + \cos [(\omega_o + 2\omega_e)t + \phi_o(t) + 2\phi_e(t)] \}. \quad (9)$$

In another approach [20], an optical notch filter is used to eliminate the optical carrier at the output of the optical phase modulator. The resulting spectrum is shown in Fig. 3(c). The

dashed arrow signifies the removal of the optical carrier. Using (8), the optical signal after the notch filter is then given by

$$E_{P2}(t) = E_o \sum_{n=-\infty}^{+\infty} J_n(\beta_p) \cos \left[(\omega_o + n\omega_e)t + \phi_o(t) + n\phi_e(t) + n\frac{\pi}{2} \right] - E_o J_0(\beta_p) \cos(\omega_o t + \phi_o(t)). \quad (10)$$

Comparing (6), (7), and (9), we obtain a general expression for the optical signal produced by the configurations based on: 1) an intensity modulator alone; 2) an intensity modulator with a notch filter to eliminate the optical carrier; and 3) a phase modulator with a Fabry–Pérot filter

$$E_{\text{out}}(t) = E_o J_n(\beta) \{ \cos [(\omega_o - n\omega_e)t + \phi_o(t) - n\phi_e(t)] + \cos [(\omega_o + n\omega_e)t + \phi_o(t) + n\phi_e(t)] \} \quad (11)$$

where β is a general representation of the modulation index β_i or β_p and n is a positive integer with $n = 1$ or $n = 2$. Optical signals expressed in (10) and (11) represent all reported approaches for harmonically generated electrical signals based on external optical modulation techniques. In the following, we will discuss the phase-noise performance of the optically generated microwave signals.

III. PHASE-NOISE REPRESENTATION OF THE ELECTRICAL DRIVE SIGNAL

A. Low-Index Approximation of the Electrical Drive Signal

Due to the intrinsic properties of the noise and the central limit theorem, the phase fluctuation $\phi_e(t)$ of the electrical signal $V(t)$ expressed by (2) is classically treated as a stationary zero-mean Gaussian random process [33]. This allows the existence of the autocorrelation function $R_{\phi_e}(\tau)$ of $\phi_e(t)$ as

$$R_{\phi_e}(\tau) = \langle \phi_e(t + \tau) \phi_e(t) \rangle \quad (12)$$

where τ is a time shift and $\langle \rangle$ represents the ensemble average. Using the Wiener–Khinchine theorem [34], the double sideband (DSB) PSD $S_{\phi_e}(f)$ of $\phi_e(t)$ can be obtained as

$$S_{\phi_e}(f) = F [R_{\phi_e}(\tau)] \quad (13)$$

where F denotes the Fourier-transform operation. Although $S_{\phi_e}(f)$ has theoretical pertinence, it is not a quantity that can be directly measured. In contrast, the SSB PSD of $V(t)$, where $V(t)$ is a random process built up from $\phi_e(t)$, can be measured by a spectrum analyzer.

Using a noise model that assumes the low-index phase modulation of $\phi_e(t)$ [35], the DSB PSD $S_{\phi_e}(f)$ of $\phi_e(t)$ has a simple relation with the measurable SSB PSD of $V(t)$. This condition is met in most practical applications in which the electrical drive signal is created by an electrical source with a high spectral quality. Under this condition, the electrical drive signal has a small phase fluctuation and $R_{\phi_e}(0) \ll 1$, i.e., the mean power of the phase fluctuation $\phi_e(t)$ is much smaller than 1 rad^2 . In the remainder of this paper, our analysis is developed under the low phase modulation index condition.

In order to obtain the expression giving the SSB PSD of $V(t)$, we have to first find the expression for its autocorrelation function. It is found that $V(t)$ is not stationary in a wide sense (WSS), although $\phi_e(t)$ is stationary [35]. However, $V(t)$ has a defined time-averaged autocorrelation function. If $R_V(\tau)$ and $S_V(f)$ are denoted as the time-averaged autocorrelation function and the SSB PSD of the electrical drive signal $V(t)$, respectively, then $R_V(\tau)$ can be obtained by using

$$R_V(\tau) = \overline{\langle V(t + \tau)V(t) \rangle} = \frac{V_e^2}{2} \cos(\omega_e \tau) \exp \{ - [R_{\phi_e}(0) - R_{\phi_e}(\tau)] \} \quad (14)$$

where $\overline{\langle f(t) \rangle}$ represents time average of $f(t)$, and τ is a time shift. Equation (14) makes use of the fact that $\phi_e(t)$ is a stationary zero-mean Gaussian random process. With the condition that $R_{\phi_e}(0) \ll 1$, generally, $R_V(\tau)$ can be further simplified as

$$R_V(\tau) \cong \frac{V_e^2}{2} \cos(\omega_e \tau) [1 - R_{\phi_e}(0) + R_{\phi_e}(\tau)]. \quad (15)$$

Using the Wiener–Khinchine theorem, the SSB $S_V(f)$ is found to be

$$S_V(f) = F [R_V(\tau)] \cong \frac{V_e^2}{2} [1 - R_{\phi_e}(0)] \delta(f - f_e) + \frac{V_e^2}{2} S_{\phi_e}(f - f_e) \quad (16)$$

where $\delta(f)$ is the impulse function, and $S_{\phi_e}(f)$ is the DSB PSD of $\phi_e(t)$. Equation (16) indicates that $S_V(f)$ is an exact replica of the DSB $S_{\phi_e}(f)$ around f_e , except that it is multiplied by the constant linear factor $V_e^2/2$. Therefore, one can use the measurable function $S_V(f)$ to represent $S_{\phi_e}(f)$ for characterizing the phase fluctuation of an electrical drive signal with high spectral quality.

B. SSB PSD and Phase-Noise Measurement of the Electrical Drive Signal

Based on circuit theory, the SSB PSD of an electrical signal produced by an oscillator can be expressed as a power series of offset frequencies [30], [33]. The overall noise of the oscillator is contributed from various types of noise, such as $1/f$ noise, shot noise, and thermal noise. Considering these, the SSB PSD of the electrical signal can be expressed as

$$S(f) = \frac{A}{|f - f_c|^2} + \frac{B}{|f - f_c|^3} \quad (17)$$

where f_c is the center frequency of the electrical signal, A and B are two constants, f is an arbitrary frequency around f_c , and $f \neq f_c$. Again, we would like to assess the relationship between the measured function $S_V(f)$ and the expression defined in (17).

To do so, we introduce another technique to evaluate the phase noise. It is based on the ratio of the power in one phase modulation sideband (on a per-Hertz basis) to the total power of the signal [36]. This new quantity is denoted as $L_V(f_m)$ and called the phase noise of the signal, where f_m represents

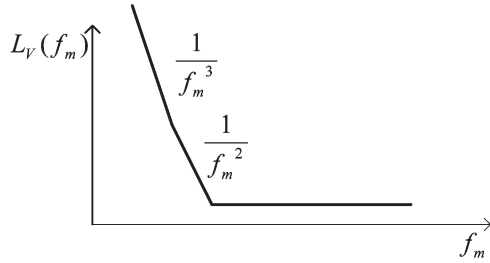


Fig. 4. Phase noise $L_V(f_m)$ in the approximation of a power of offset frequency.

a frequency shift from the carrier frequency f_e . It can be demonstrated that $L_V(f_m)$ can be expressed as a function of $S_V(f)$ by using

$$\begin{aligned} L_V(f_m) &= \frac{P_{\text{SSB}}(f_e + f_m, 1 \text{ Hz})}{P_e} \\ &\simeq \frac{S_V(f_e + f_m)}{P_e} \\ &= \frac{1}{P_e} \left[\frac{A}{f_m^2} + \frac{B}{f_m^3} \right] \end{aligned} \quad (18)$$

where $P_e = V_e^2/2$ is the average power of the electrical signal expressed in (2) and $f_m > 0$. Therefore, $L_V(f_m)$ is proportional to $S_V(f)$, the proportionality constant being the inverse of the average power in $V(t)$. A typical plot of $L_V(f_m)$ is shown in Fig. 4. Finally, we conclude that the PSD of $V(t)$ completely describes the phase noise of the electrical signal. Hence, in the remainder of this paper, the analysis will be focused on the evaluation of the PSDs of the optically generated electrical signals.

The singularity of the SSB PSD expressed in (17) does not allow us to perform an inverse Fourier transform to obtain its autocorrelation function. However, based on (13), (16), and (17), we can loosely denote that

$$S_{\phi_e}(f) = F[R_{\phi_e}(\tau)] \simeq \frac{1}{P_e} \left[\frac{A}{|f|^2} + \frac{B}{|f|^3} \right] \quad (19)$$

where $f \neq 0$.

IV. PHASE-NOISE ANALYSIS OF THE LOCALLY GENERATED MICROWAVE SIGNALS

When the optical signal expressed in (10) or (11) is fed into a square-law photodetector, electrical signals will be generated. For the optical signal defined in (10), the generated high-frequency electrical signal $V_{P2}(t)$ can be written as

$$V_{P2}(t) = C_1 \sum_{n=1}^{+\infty} J_0(\beta_p) J_{2n}(\beta_p) \cos[2n\omega_e t + 2n\phi_e(t) + n\pi] \quad (20)$$

where C_1 is a constant related to the value of E_o and the responsivity of the photodetector, and the property of the Bessel function $J_{-n}(\beta_p) = (-1)^n J_n(\beta_p)$ is used. Equation (20) clearly indicates that only even-order harmonics of the electrical drive signal are generated [20]. Equation (20) also

shows that the phase fluctuation of the generated electrical harmonics is not affected by the phase fluctuation $\phi_o(t)$ of the optical carrier. This is because there is a complete correlation between the noises presented at the sidebands defined by (10), since the light feeding the modulator comes from a single light source. Therefore, complete noise cancellation occurs after photo-detection. Thus, the phase fluctuation of the optical source will not contribute to the phase noise of the generated electrical signal. Similarly, for the optical signal expressed in (11), the generated high-frequency electrical signal is

$$V_{\text{out}}(t) = C_1 J_n^2(\beta) \cos[2n\omega_e t + 2n\phi_e(t)] \quad (21)$$

where C_1 is defined as before.

Concentrating on one of the harmonics defined in (20) and (21) enables us to use a common mathematical expression for $V_{P2}(t)$ and $V_{\text{out}}(t)$:

$$V_L(t) = C_L \cos[2n\omega_e t + 2n\phi_e(t)] \quad (22)$$

where C_L is a constant.

Applying the theory developed in Section III-A, the autocorrelation function of $V_L(t)$ is found to be

$$R_{V_L}(\tau) \simeq \frac{C_L^2}{2} \cos(2n\omega_e \tau) [1 - (2n)^2 R_{\phi_e}(0) + (2n)^2 R_{\phi_e}(\tau)] \quad (23)$$

and the SSB PSD of $V_L(t)$ is

$$\begin{aligned} S_{V_L}(f) &= F[R_{V_L}(\tau)] \\ &\simeq \frac{C_L^2}{2} [1 - (2n)^2 R_{\phi_e}(0)] \delta(f - 2nf_e) \\ &\quad + \frac{C_L^2}{2} (2n)^2 S_{\phi_e}(f - 2nf_e). \end{aligned} \quad (24)$$

Using (19) to express $S_{\phi_e}(f)$ in the form of $L_V(f_m)$, we obtain a closed-form expression of the SSB PSD of the locally generated electrical signal

$$\begin{aligned} S_{V_L}(f) &\simeq \frac{C_L^2}{2} [1 - (2n)^2 R_{\phi_e}(0)] \delta(f - 2nf_e) \\ &\quad + \frac{C_L^2}{2} (2n)^2 \frac{1}{P_e} \left[\frac{A}{|f - 2nf_e|^2} + \frac{B}{|f - 2nf_e|^3} \right]. \end{aligned} \quad (25)$$

Because the total average power of $V_L(t)$ is $C_L^2/2$, the SSB phase noise $L_{V_L}(f_m)$ of $V_L(t)$ is then given by

$$\begin{aligned} L_{V_L}(f_m) &= \frac{S_{V_L}(2nf_e + f_m)}{C_L^2/2} \\ &\simeq (2n)^2 \frac{1}{P_e} \left[\frac{A}{|f_m|^2} + \frac{B}{|f_m|^3} \right] \end{aligned} \quad (26)$$

where f_m is the offset frequency away from $2nf_e$.

It is clear that $L_{V_L}(f_m)$ in (26) is $(2n)^2$ times $L_V(f_m)$ in (18). It shows that the phase noise of the locally generated electrical signal has a $20 \log(2n)$ (dB) degradation with respect to the phase noise of the electrical drive signal, where $2n$ is the frequency multiplication number. This is exactly the same result

as would be obtained for an electronic frequency multiplier [37]. Due to the absence of the transmission fiber, in the optical sidebands, the phase noises originated from the optical source are fully correlated. They canceled in the beating process. Therefore, the phase noise of the locally generated electrical is immunized to the phase noise of the optical source.

V. PHASE-NOISE ANALYSIS OF THE REMOTELY GENERATED ELECTRICAL SIGNALS

The phase noise present in the sidebands of the optical carrier is fully correlated. Therefore, the phase noise of the locally generated electrical signal can be much lower than that of the optical source. However, when these optical signals, as expressed in (10) and (11), are transmitted over SSMF, different time delays will be introduced to the various optical sidebands at the output of the system because of chromatic dispersion. If the frequency of an optical sideband is nf_e , the time-delay difference (τ_D) between the n th-order sideband and the optical carrier at the end of the span is given by

$$\tau_D = DL\delta\lambda = -n\tau_d \quad (27)$$

where

$$\tau_d = \frac{DL\lambda_0^2 f_e}{c} \quad (28)$$

τ_d is the fundamental time-delay difference between the first-order sideband and the optical carrier, D is the chromatic-dispersion parameter of the fiber [typically 17 ps/(nm · km) at 1550 nm for SSMF], L is the length of the fiber, $\delta\lambda$ is the wavelength difference between the optical carrier and the n th-order optical sideband, λ_0 is the center wavelength of the optical source, c is the speed of light in free space, and n is the sideband order.

For the optical signal defined in (11), the expression for the optical signal at the end of the link is

$$\begin{aligned} E_2(t) = & \alpha E_o J_n(\beta) \cos [(\omega_o - n\omega_e)(t - n\tau_d) \\ & + \phi_o(t - n\tau_d) - n\phi_e(t - n\tau_d)] \\ & + \alpha E_o J_n(\beta) \cos [(\omega_o + n\omega_e)(t + n\tau_d) \\ & + \phi_o(t + n\tau_d) + n\phi_e(t + n\tau_d)] \end{aligned} \quad (29)$$

where $E_2(t)$ represents the output signal when the input signal is $E_{out}(t)$ in (11). Also, α is the attenuation of the fiber.

We now express the electrical signal generated from the optical signal defined in (29)

$$\begin{aligned} V_R(t) = & C_R \cos \{2n\omega_e t + 2n\omega_o \tau_d \\ & + n[\phi_e(t + n\tau_d) + \phi_e(t - n\tau_d)] \\ & + \phi_o(t + n\tau_d) - \phi_o(t - n\tau_d)\} \end{aligned} \quad (30)$$

where C_R is a constant, which is related to values α , E_o , $J_n(\beta)$, and the responsivity of the photodetector. Equation (30) shows that the phase fluctuation of the remotely generated electrical

signal depends on the fiber chromatic dispersion and the phase fluctuations of the electrical drive signal and optical carrier.

$V_R(t)$, like $V(t)$, is not a WSS random process. The time-averaged autocorrelation function of $V_R(t)$, which is denoted by $R_{V_R}(\tau)$, is given by

$$\begin{aligned} R_{V_R}(\tau) = & \overline{\langle V_R(t + \tau)V_R(t) \rangle} \\ = & \frac{C_R^2}{2} \cos(2n\omega_e \tau) \\ & \times \langle \cos \{n[\phi_e(t + n\tau_d + \tau) - \phi_e(t + n\tau_d) \\ & + \phi_e(t - n\tau_d + \tau) - \phi_e(t - n\tau_d)]\} \rangle \\ & \times \langle \cos [\phi_o(t + n\tau_d + \tau) - \phi_o(t + n\tau_d) \\ & - \phi_o(t - n\tau_d + \tau) + \phi_o(t - n\tau_d)] \rangle \end{aligned} \quad (31)$$

where $\overline{f(t)}$, $\langle \cdot \rangle$, and τ are defined as before. The independent property of $\phi_o(t)$ and $\phi_e(t)$, and the zero-mean Gaussian property of $\phi_o(t)$ and $\phi_e(t)$ are used in obtaining (31). To better understand the contribution of each factor to the phase noise of the remotely generated electrical signal, $R_{V_R}(\tau)$ can be rewritten as

$$R_{V_R}(\tau) = \frac{C_R^2}{2} \cos(2n\omega_e \tau) R_{e,R}(\tau) R_{o,R}(\tau) \quad (32)$$

where

$$\begin{aligned} R_{e,R}(\tau) = & \langle \cos \{n[\phi_e(t + n\tau_d + \tau) - \phi_e(t + n\tau_d) \\ & + \phi_e(t - n\tau_d + \tau) - \phi_e(t - n\tau_d)]\} \rangle \end{aligned} \quad (33)$$

and

$$\begin{aligned} R_{o,R}(\tau) = & \langle \cos [\phi_o(t + n\tau_d + \tau) - \phi_o(t + n\tau_d) \\ & - \phi_o(t - n\tau_d + \tau) + \phi_o(t - n\tau_d)] \rangle \end{aligned} \quad (34)$$

where $R_{e,R}(\tau)$ and $R_{o,R}(\tau)$ are the electrical and optical autocorrelation functions of $V_R(\tau)$, respectively. If $S_{V_R}(f)$ is denoted as the SSB PSD of $V_R(t)$, $S_{e,R}(f)$, and $S_{o,R}(f)$ are denoted as the Fourier transforms of $R_{e,R}(\tau)$ and $R_{o,R}(\tau)$, respectively, then

$$\begin{aligned} S_{V_R}(f) = & F [R_{V_R}(\tau)] \\ = & \frac{C_R^2}{2} \delta(f - 2nf_e) * S_{e,R}(f) * S_{o,R}(f) \end{aligned} \quad (35)$$

where $*$ is the convolution operator. $S_{e,R}(f)$ and $S_{o,R}(f)$ are the DSB PSD of the electrical and optical contributions to $S_{V_R}(f)$, respectively. They are investigated separately in the following two sections.

A. Electrical Driving Signal Contribution to the SSB PSD of the Remotely Generated Electrical Signal

Based on the assumption that $\phi_e(t)$ is stationary and on the spectral quality of the electrical drive signal discussed in

Section III-A, the low phase modulation index approximation is used again to simplify the expression of $R_{e,R}(\tau)$ in (33). $R_{e,R}(\tau)$ can then be expressed as a function of $R_{\phi_e}(\tau)$:

$$R_{e,R}(\tau) \cong 1 - 2n^2 [R_{\phi_e}(0) + R_{\phi_e}(2n\tau_d)] + n^2 [2R_{\phi_e}(\tau) + R_{\phi_e}(\tau + 2n\tau_d) + R_{\phi_e}(\tau - 2n\tau_d)]. \quad (36)$$

Then, $S_{e,R}(f)$ is found to be

$$S_{e,R}(f) = F[R_{e,R}(\tau)] \cong \{1 - 2n^2 [R_{\phi_e}(0) + R_{\phi_e}(2n\tau_d)]\} \delta(f) + (2n)^2 \cos^2(2n\pi\tau_d f) \frac{1}{P_e} \left[\frac{A}{|f|^2} + \frac{B}{|f|^3} \right]. \quad (37)$$

We have used the expression for $S_{\phi_e}(f)$ given in (19) to obtain (37).

Note that when $\tau_d = 0$, (37) becomes identical to (25) if the constant amplitude and frequency shift are ignored. That means that the DSB PSD expression in (37) is more general for characterizing the phase noise of the optically generated electrical signal.

Typical plots of $S_{e,R}(f)/S_{\phi_e}(f)$ in decibel for frequency greater than zero are shown in Fig. 5.

B. Optical Carrier Contribution to the SSB PSD of the Remotely Generated Electrical Signal

The phase fluctuation of the optical carrier expressed in (1) is characterized by a Wiener-Lévy process [39], i.e.,

$$\phi_o(t) = 2\pi \int_0^t F(\tau) d\tau \quad (38)$$

where $F(t)$ is a white Gaussian random process characterizing the frequency noise in a laser source. The PSD of $F(t)$ is a constant N_0 . The PSD of the noisy carrier $E(t) = \exp[j\phi_o(t)]$, which is denoted $S_E(f)$, turns out to be Lorentzian in shape [39]

$$S_E(f) = \frac{2}{\pi B} \frac{1}{1 + \left(\frac{2f}{B}\right)^2} \quad (39)$$

where $B = 2\pi N_0$ denotes the two-sided half-power bandwidth.

It is clear that the Wiener-Lévy process $\phi_o(t)$ expressed in (38) is a nonstationary zero-mean Gaussian process and is not periodic with respect to time. Hence, the time average technique that we used earlier for obtaining the autocorrelation functions of $V(t)$ and $V_L(t)$ cannot be used here. Without the autocorrelation function of $\phi_o(t)$, the low-index approximation treatment cannot be used for the analysis of $S_{o,R}(f)$.

However, one interesting property of the statistical distribution given in (38) is that all phase fluctuations over nonoverlapping time periods are statistically independent [34]. This

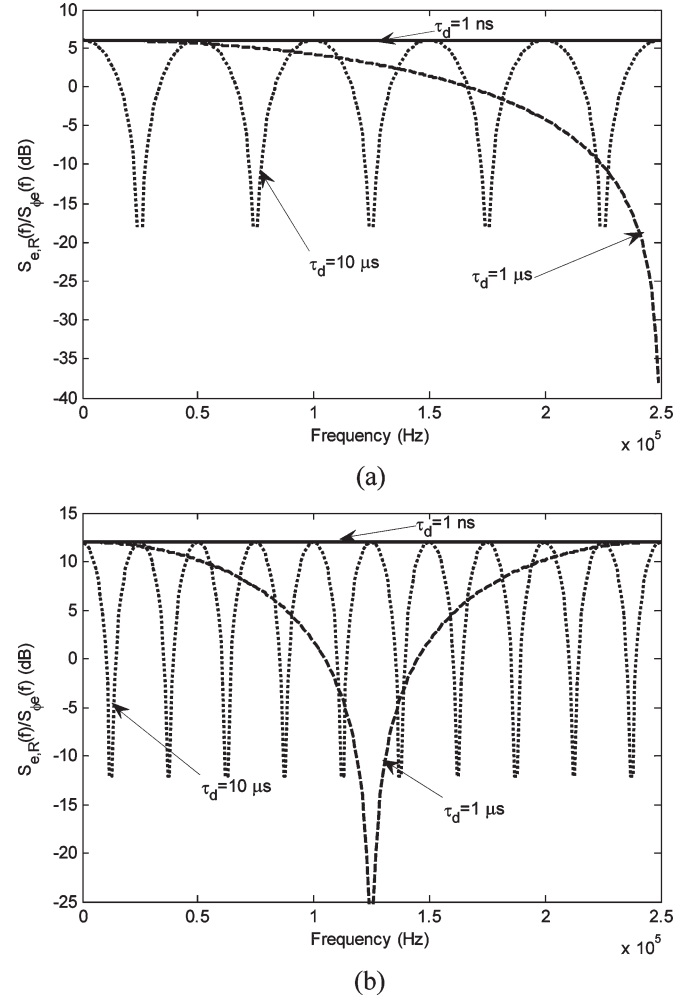


Fig. 5. Plots of $S_{e,R}(f)/S_{\phi_e}(f)$. (a) $n = 1$. (b) $n = 2$.

allows us to obtain an expression of $S_{o,R}(f)$ from $R_{o,R}(\tau)$ in (35). $S_{o,R}(f)$ is

$$S_{o,R}(f) = \exp\left[-\frac{4n\tau_d}{\tau_c}\right] \left\{ \delta(f) + \frac{\tau_c}{1 + (\pi f \tau_c)^2} \times \left\{ \exp\left[\frac{4n\tau_d}{\tau_c}\right] - \cos(4n\pi f \tau_d) + \pi f \tau_c \sin(4n\pi f \tau_d) \right\} - \frac{\sin(4n\pi f \tau_d)}{\pi f} \right\} \quad (40)$$

where τ_c is the coherence time of the optical carrier [40], and

$$\tau_c = \frac{1}{\pi B}. \quad (41)$$

The derivation of (40) is given in the Appendix.

Typical plots of $S_{o,R}(f)$ in decibel meters are shown in Fig. 6, where the 3-dB linewidth of the laser source is 10 MHz.

Substitute (37) and (40) into (35), we obtain the closed-form expression of $S_{V_R}(f)$ as

$$\begin{aligned}
 S_{V_R}(f) = & \frac{C_R^2}{2} \exp\left[-\frac{4n\tau_d}{\tau_c}\right] \delta(f - 2nf_e) \\
 & * \left\{ \left\{ 1 - 2n^2 [R_{\phi_e}(0) + R_{\phi_e}(2n\tau_d)] \right\} \delta(f) \right. \\
 & + (2n)^2 \cos^2(2n\pi\tau_d f) \frac{1}{P_e} \left[\frac{A}{|f|^2} + \frac{B}{|f|^3} \right] \\
 & + \left\{ 1 - 2n^2 [R_{\phi_e}(0) + R_{\phi_e}(2n\tau_d)] \right\} \\
 & \times \left\{ \frac{\tau_c}{1 + (\pi\tau_c f)^2} \left\{ \exp\left[\frac{4n\tau_d}{\tau_c}\right] - \cos(4n\pi\tau_d f) \right. \right. \\
 & \quad \left. \left. + \pi\tau_c f \sin(4n\pi\tau_d f) \right\} \right. \\
 & \quad \left. - \frac{\sin(4n\pi\tau_d f)}{\pi f} \right\} \\
 & + (2n)^2 \cos^2(2n\pi\tau_d f) \frac{1}{P_e} \left[\frac{A}{|f|^2} + \frac{B}{|f|^3} \right] \\
 & * \left\{ \frac{\tau_c}{1 + (\pi\tau_c f)^2} \left\{ \exp\left[\frac{4n\tau_d}{\tau_c}\right] - \cos(4n\pi\tau_d f) \right. \right. \\
 & \quad \left. \left. + \pi f \tau_c \sin(4n\pi\tau_d f) \right\} \right. \\
 & \quad \left. - \frac{\sin(4n\pi\tau_d f)}{\pi f} \right\} \left. \right\} \quad (42)
 \end{aligned}$$

where $*$ is the convolution operator. If the SSB phase noise of the remotely generated electrical signal is denoted as $L_{V_R}(f_m)$, the expression of $L_{V_R}(f_m)$ obtained from $S_{V_R}(f)$ is

$$\begin{aligned}
 L_{V_R}(f_m) \approx & (2n)^2 \cos^2(2n\pi\tau_d f_m) \frac{1}{P_e} \left[\frac{A}{|f_m|^2} + \frac{B}{|f_m|^3} \right] \\
 & + \frac{\tau_c}{1 + (\pi\tau_c f_m)^2} \left\{ \exp\left[\frac{4n\tau_d}{\tau_c}\right] - \cos(4n\pi\tau_d f_m) \right. \\
 & \quad \left. + \pi\tau_c f_m \sin(4n\pi\tau_d f_m) \right\} \\
 & - \frac{\sin(4n\pi\tau_d f_m)}{\pi f_m} + (2n)^2 \cos^2(2n\pi\tau_d f_m) \\
 & \times \frac{1}{P_e} \left[\frac{A}{|f_m|^2} + \frac{B}{|f_m|^3} \right] \\
 & * \left\{ \frac{\tau_c}{1 + (\pi\tau_c f_m)^2} \left\{ \exp\left[\frac{4n\tau_d}{\tau_c}\right] - \cos(4n\pi\tau_d f_m) \right. \right. \\
 & \quad \left. \left. + \pi\tau_c f_m \sin(4n\pi\tau_d f_m) \right\} \right. \\
 & \quad \left. - \frac{\sin(4n\pi\tau_d f_m)}{\pi f_m} \right\} \quad (43)
 \end{aligned}$$

where f_m is the offset frequency away from $2nf_e$, and $f_m \neq 0$. In (43), the approximation of $1 - 2n^2 [R_{\phi_e}(0) + R_{\phi_e}(2n\tau_d)] \approx 1$ is used.

Because of the singularity of (42) and (43) at f and $f_m = 0$, their convolution cannot be conducted analytically. This

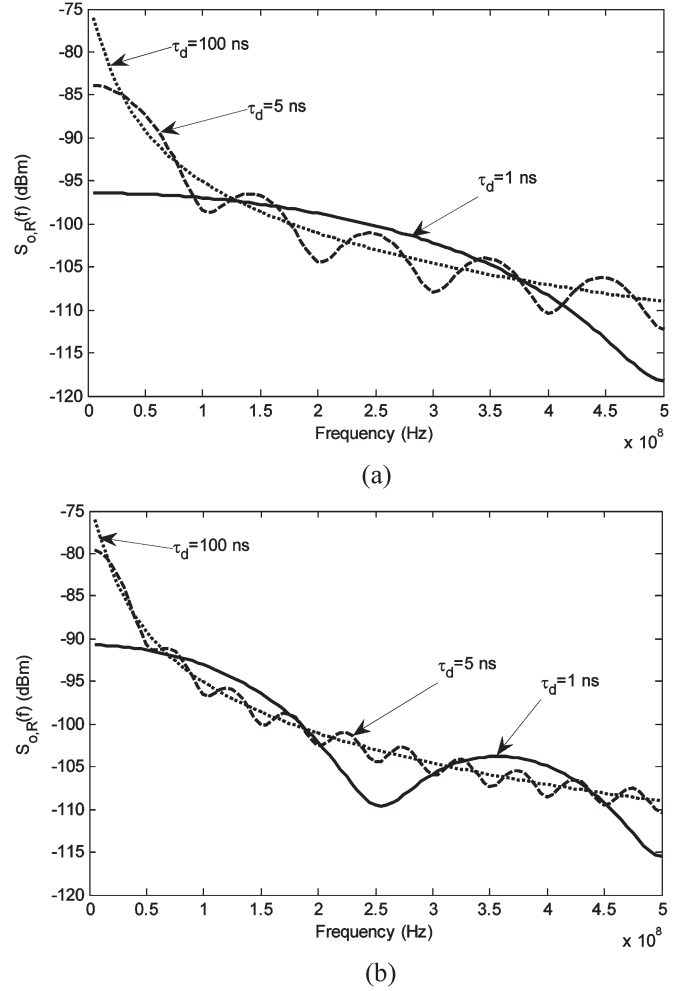


Fig. 6. Plots of $S_{e,R}(f)$ for $B = 10$ MHz. (a) $n = 1$. (b) $n = 2$.

problem can be alleviated by using the processed data from an electrical spectrum measurement of the drive signal $V_e(t)$ to represent $(1/P_e)[(A/|f_m|^2) + (B/|f_m|^3)]$ in (42) and (43). Then, based on (16), $S_{V_e}(f)$ can be changed to $S_{\phi_e}(f)$. Here, the resolution bandwidth (RBW) of the spectrum analyzer has to be set to 1 Hz or converted to the 1-Hz basis when obtaining the SSB PSD of $V_e(t)$.

For the optical signal expressed by (10), analyses showed that a dispersion compensation module (DCM) is needed to alleviate the power variation problem of the generated electrical signal [38]. With the deployment of the DCM, the time-delay difference caused by the chromatic dispersion is fully compensated. Then, the phase noise of the remotely generated electrical signals is exactly the same as that of the signal generated locally.

VI. EXPERIMENT

A. Experiment with a Tunable Laser Source

To validate the above analysis, an experimental setup shown in Fig. 7 is built. In the setup, a tunable laser source with two linewidth settings is used to investigate the phase-noise performance of the generated electrical signals with different optical carrier linewidths.

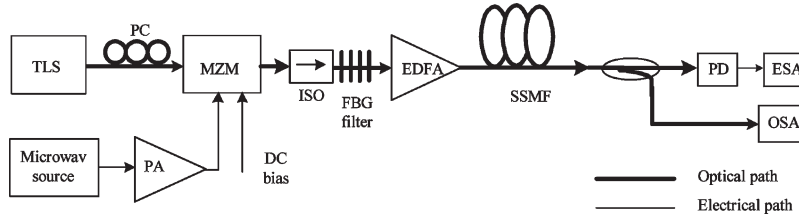


Fig. 7. Experimental setup for optical generation and transmission of mm-wave signals (TLS, tunable laser source; PC, polarization controller; MZM, Mach-Zehnder modulator; ISO, isolator; EDFA, erbium-doped fiber amplifier; PA, power amplifier; OSA, optical spectrum analyzer; PD, photodetector; ESA, electrical spectrum analyzer; SSMF, standard single mode fiber).

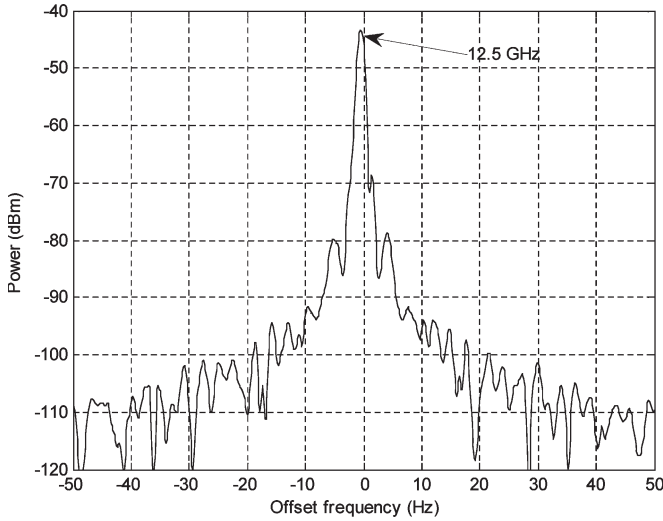


Fig. 8. Electrical spectrum of the electrical drive signal at 12.5 GHz.

The electrical signal is generated by externally modulating the optical carrier with an electrical drive signal via an optical intensity modulator. Odd-order optical sidebands are suppressed with a constant dc bias. The optical carrier is filtered out with a narrowband optical FBG filter. Two second-order optical sidebands remain at the output of the FBG filter when the power of the electrical drive signal is balanced with the attenuation of the FBG filter. This experimental setup supports the generation of a continuously tunable millimeter-wave signal with a frequency of four times that of the electrical drive signal. The advantage of this configuration is that the wavelength of the optical carrier is fixed; therefore, a tunable optical notch filter is not required to remove the optical carrier.

The tunable laser source used in Fig. 7 is an Anritsu MG9637A. It has two optical linewidth settings of 700 kHz and 50 MHz, corresponding to coherence times of $\tau_{c1} = 455$ ns and $\tau_{c2} = 6.37$ ns, respectively. The SSMF used in Fig. 7 has a chromatic dispersion of 17 ps/(nm · km). Fibers with lengths of 25 and 50 km are used in the experiment. When the wavelength of the optical carrier is 1543 nm and the frequency of the electrical drive signal is 12.5 GHz, from (28), the fundamental time-delay differences of the 25- and 50-km fibers are $\tau_{d1} = 0.04216$ ns and $\tau_{d2} = 0.08432$ ns, respectively. The spectrum of the electrical drive signal at 12.5 GHz is shown in Fig. 8. The spectral measurement is performed with an HP8565E electrical spectrum analyzer, which is set to an RBW of 1 Hz and a frequency span of 100 Hz. The phase noise is measured to be -48 dBc/Hz @ 10 Hz.

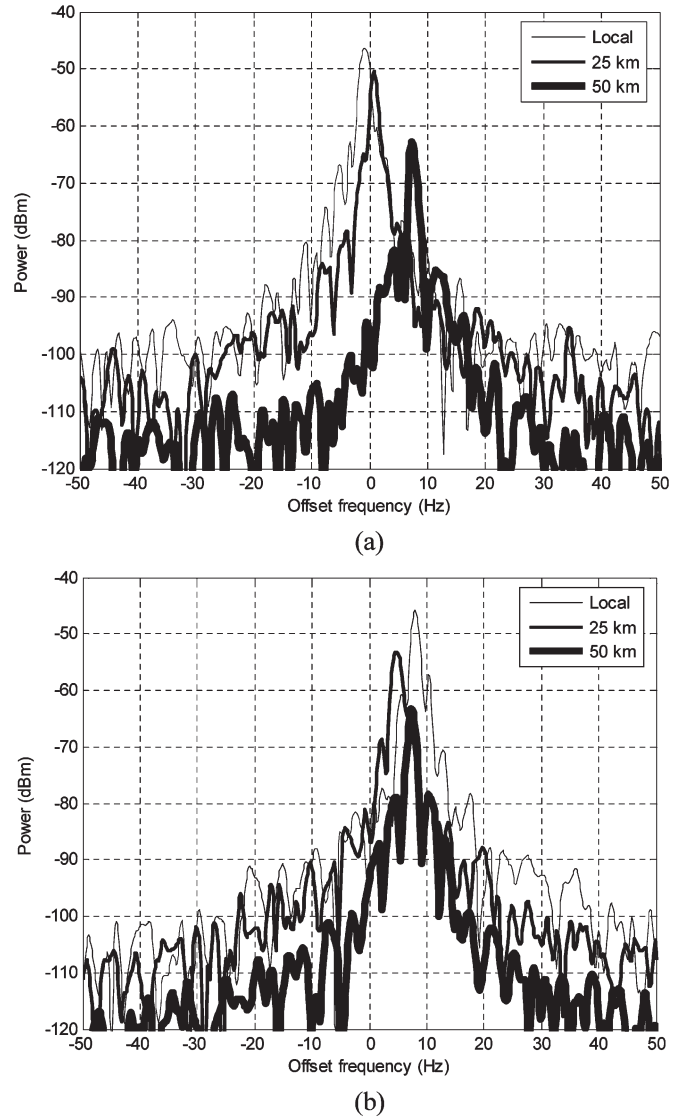


Fig. 9. Spectra of the locally and remotely generated electrical signals at 50 GHz. (a) The linewidth of the optical signal is set at 700 kHz. (b) The linewidth of the optical signal is set at 50 MHz.

Fig. 9 shows the spectra of the locally and remotely generated electrical signals at 50 GHz when the linewidths of the optical carrier are respectively set at 700 kHz and 50 MHz, with fiber lengths of 0, 25, and 50 km. For locally generated 50-GHz signals, the phase noises are -35.5 dBc/Hz @ 10 Hz for the two different carrier linewidths, as shown in Fig. 9(a) and (b). Compared with the phase noise of the drive signal shown in Fig. 8, the phase-noise degradation is very close

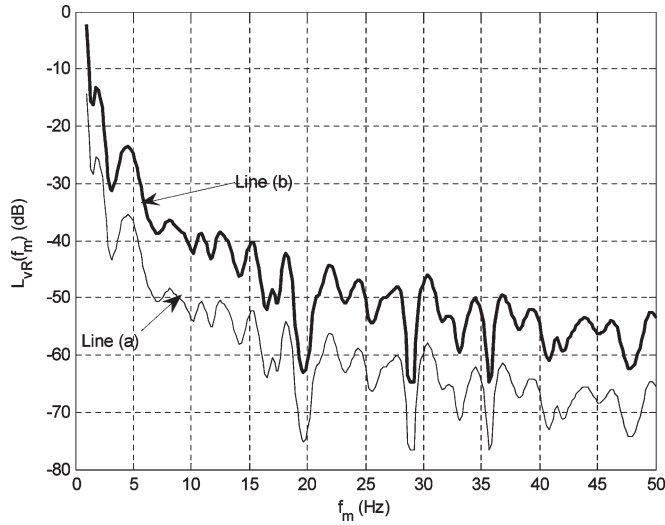


Fig. 10. Electrical spectrum of the 12.5-GHz electrical drive signal (line a) and simulated spectra of the locally and remotely generated electrical signals at 50 GHz (line b). There is no visible deviation in the simulated results.

to the theoretical value of 12 dB. The measurement agrees with the prediction given by (26) in Section IV. For remotely generated 50-GHz signals, a negligible phase-noise degradation is observed for the two different carrier linewidths with two different transmission distances, as shown in Fig. 9(a) and (b). This is in good agreement with the analytical predictions of (43), as shown in the simulated spectral plots in Fig. 10.

In Fig. 10, line (a) is the normalized spectrum of the 12.5-GHz electrical drive signal obtained from the experimental measurement. Line (b) consists of five simulated spectra of the 50-GHz signals generated locally and remotely. For the locally generated signal, the spectrum in line (b) is obtained from (26). For the remotely generated signals, the spectra in line (b) are obtained from (43). In the simulation of (43), the phase noise of the electrical drive signal $(1/P_e)[(A/|f_m|^2) + (B/|f_m|^3)]$ is substituted with the experimental data obtained from spectrum measurement; and the coherence time of the optical source of 700 kHz and 50 MHz and the delay time difference of the transmission fiber of 25 and 50 km are simulated. All five spectra overlap on line (b), showing that there is negligible phase-noise degradation for the five different situations. The experimental measurement shown in Fig. 9 agrees with the theoretical prediction given by (43) in Fig. 10.

Note that the deviation in the peak frequency offset in Fig. 9 is caused by the frequency fluctuations of the electrical drive signal at 12.5 GHz. The amplitude offset is attributed to the fiber loss. In addition, using an electrical spectrum analyzer (Agilent 8565E) to measure the phase noise is an approximate technique, and the total frequency span is limited when using a 1-Hz RBW. Phase noise at larger offset frequencies will decrease monotonically.

B. Experiment with a Sliced ASE Source

To further investigate the impact of the linewidth of the optical carrier and the transmission distance on the phase-noise performance of the remotely generated electrical signal, the

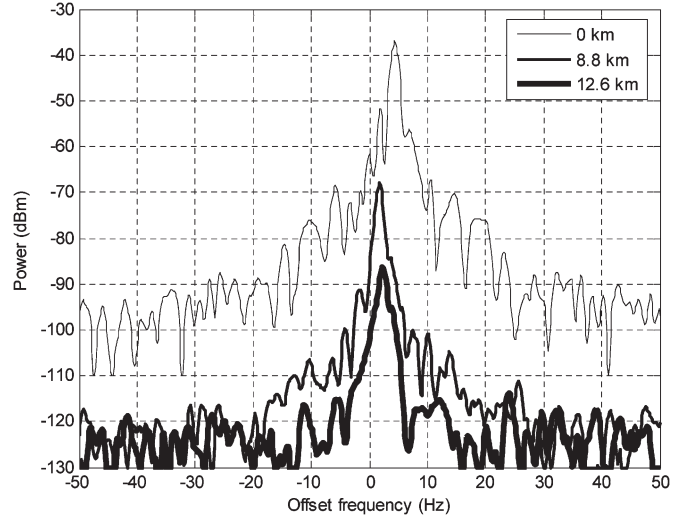


Fig. 11. Electrical spectra of the locally and remotely generated electrical signal at 50 GHz using a sliced ASE source with a linewidth of 33 GHz.

tunable laser source in Fig. 7 is replaced by a sliced ASE source obtained by slicing an EDFA ASE noise with an FBG. The FBG has a 3-dB bandwidth of 33 GHz. As a rough approximation, the linewidth of the sliced ASE source is assumed to equal the bandwidth of the FBG. It should be noted that the PSD of the sliced ASE source does not follow a Lorentzian shape; hence the experimental results obtained are an approximation of the analysis.

The experiment using the sliced ASE source is performed with fiber transmission lengths of 0, 8.8, and 12.6 km. Their spectra are shown in Fig. 11. As can be seen, there is negligible phase-noise difference between the generated electrical signals after 0- and 8.8-km transmission. For these two lengths, the main degradation comes from an important power loss of the overall signal. This loss is much larger than what would be expected when taking into account the fiber loss only. For the 12.6-km spectrum, the signal power at the offset frequency of 10 Hz is within the system noise floor due to the large power drop of the generated electrical signal. Adequate phase-noise measurement could not be conducted. The power drop of the generated electrical signal over the SSMF transmission is indicated by the first term of (42).

To further study the phase-noise degradation versus the fiber transmission length with the sliced ASE source, we simulate the spectra of the generated electrical signal using (43) for fiber transmission lengths of 0, 10, 12, 14, 16, and 18 km. The simulation results are shown in Fig. 12. As can be seen, when the transmission distance is below 10 km, there is negligible phase-noise degradation, which is consistent with the experimental result in Fig. 11. When the transmission distance is over 12 km at the offset frequency of 10 Hz, the phase-noise degradation starts.

Note that there is some discrepancy between the experimental result and the simulation result, which may be caused by the limitation of the approximation of the sliced ASE source as a laser source, the inaccuracy of the 3-dB linewidth of the slicing FBG, and the inaccuracy of the fiber transmission distance.

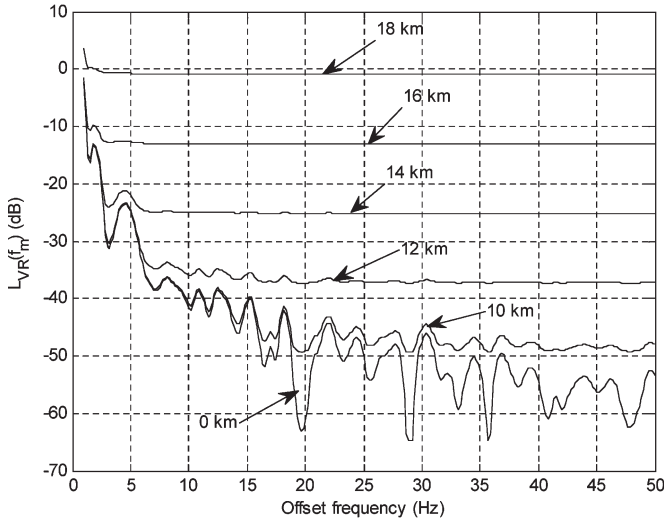


Fig. 12. Simulated spectra of the generated electrical signal at 50 GHz for different transmission lengths using the sliced ASE source with a linewidth of 33 GHz.

VII. CONCLUSION

In this paper, we have investigated theoretically and experimentally the phase-noise performance of optically generated electrical signals based on optical external-modulation techniques. Mathematical expressions for the optical signals before photodetection have been developed that incorporate the phase fluctuations of both the electrical drive signal and the optical carrier. Closed-form expressions of the PSD of the electrical signals, generated both locally and remotely, have been developed. It is shown that the PSD of the locally generated electrical signal is only determined by the phase noise of the electrical drive signal and the order of frequency multiplication. The phase-noise degradation of the locally generated electrical signal follows the same rule as in a standard electronic frequency multiplier. The PSD of the remotely generated electrical signal is additionally affected by the linewidth of the optical carrier and the chromatic-dispersion effect of the transmission fiber. Outcomes of the analysis have been validated by the experiments using a tunable laser source with optical linewidths of 700 kHz and 50 MHz and a sliced ASE source with a linewidth of 33 GHz. For the experiment using a tunable laser source with 700-kHz and 50-MHz linewidths, the phase noise of the locally generated electrical signal has a 12.5-dB degradation compared with that of the electrical drive signal. There was no significant degradation of the phase noise when this signal was generated after a 50-km SSMF transmission. For the experiment using a sliced ASE source with a linewidth of 33 GHz, no phase-noise degradation was observed when the transmission distance was within 8.8 km. When the transmission distance is 12.6 km, due to the large power drop and system sensitivity limitation, adequate phase-noise measurement cannot be conducted. However, its power degradation can be predicted by the analysis result.

The results obtained here provide a model for predicting the effect of the fiber chromatic dispersion and the linewidth of the optical source on the spectral quality of the generated electrical signal. In addition, the experimental results show when the linewidth of the optical source is within 50 MHz

and transmission distance is within 50 km; the fiber chromatic dispersion and the linewidth of the light source will cause negligible degradation to the phase noise of the optically generated electrical signal.

APPENDIX

In this Appendix, we develop the expression for $S_{o,R}(f)$ used in Section V-B from the function $R_{o,R}(\tau)$.

For a laser source, the DSB PSD of its noisy carrier $E(t) = \exp[j\phi_o(t)]$ is Lorentzian [39]. Its normalized DSB PSD is given by (39) if the autocorrelation function of $E(t)$ is denoted as $R_E(\tau)$. From (39), $R_E(\tau)$ can be obtained by the inverse Fourier transform of $S_E(f)$ as

$$\begin{aligned} R_E(\tau) &= F^{-1} [S_E(f)] \\ &= \exp \left[-\frac{|\tau|}{1/(\pi B)} \right] \\ &= \exp \left[-\frac{|\tau|}{\tau_c} \right] \end{aligned} \quad (45)$$

where F^{-1} denotes the inverse Fourier-transform operation. In addition, from the expression of $E(t)$, $R_E(\tau)$ can be obtained as

$$\begin{aligned} R_E(\tau) &= \langle E(t+\tau)E(t)^* \rangle \\ &= \langle \exp \{ j[\phi_o(t+\tau) - \phi_o(t)] \} \rangle \end{aligned} \quad (46)$$

where $E(t)^*$ is the conjugate of $E(t)$. If the increment process of $\phi_o(t)$ is denoted as $\Phi_o(t)$, i.e.,

$$\Phi_o(t) = \phi_o(t_1 + t) - \phi_o(t_1). \quad (47)$$

Obviously, $\Phi_o(t)$ is a zero-mean Gaussian processes, and random variables of $\Phi_o(t)$ are statistically independent for variables t generated by nonoverlapping time periods of $\phi_o(t)$ [34]. Using the property of Gaussian processes, (46) can be further written as

$$R_E(\tau) = \exp \left[-\frac{1}{2} \langle [\Phi_o(\tau)]^2 \rangle \right]. \quad (48)$$

From (45) and (48), the variance of the phase change process $\Phi_o(t)$ at time difference τ is

$$\langle [\Phi_o(\tau)]^2 \rangle = \frac{2|\tau|}{\tau_c}. \quad (49)$$

We rewrite $R_{o,R}(\tau)$ from (34) as

$$\begin{aligned} R_{o,R}(\tau) &= \langle \cos [\phi_o(t+n\tau_d+\tau) - \phi_o(t+n\tau_d) \\ &\quad - \phi_o(t-n\tau_d+\tau) + \phi_o(t-n\tau_d)] \rangle. \end{aligned} \quad (50)$$

When $|\tau| \leq 2n\tau_d$

$$\begin{aligned} R_{o,R}(\tau) &= \langle \cos [\phi_o(t+n\tau_d+\tau) - \phi_o(t+n\tau_d)] \\ &\quad \times \langle \cos [\phi_o(t-n\tau_d+\tau) - \phi_o(t-n\tau_d)] \rangle \\ &= \langle \cos [\Phi_o(\tau)] \rangle^2 \\ &= \exp \left[-\langle [\Phi_o(\tau)]^2 \rangle \right] \\ &= \exp \left[-\frac{2|\tau|}{\tau_c} \right]. \end{aligned} \quad (51)$$

When $|\tau| > 2n\tau_d$

$$\begin{aligned}
 R_{o,R}(\tau) &= \langle \cos [\phi_o(t + n\tau_d + \tau) - \phi_o(t - n\tau_d + \tau)] \rangle \\
 &\quad \times \langle \cos [\phi_o(t + n\tau_d) - \phi_o(t - n\tau_d)] \rangle \\
 &= \langle \cos [\Phi_o(2n\tau_d)] \rangle^2 \\
 &= \exp \left[- \left\langle [\Phi_o(2n\tau_d)]^2 \right\rangle \right] \\
 &= \exp \left[- \frac{4n\tau_d}{\tau_c} \right]. \tag{52}
 \end{aligned}$$

In the above calculations, the following relations are used [41]. If X is a zero-mean Gaussian random variable, then

$$\langle \cos(X) \rangle = \exp \left[- \frac{1}{2} \langle X^2 \rangle \right] \tag{53}$$

$$\langle \sin(X) \rangle = 0. \tag{54}$$

Then, $S_{o,R}(f)$ can be obtained as

$$\begin{aligned}
 S_{o,R}(f) &= \int_{-\infty}^{+\infty} R_{o,R}(\tau) \exp(-j2\pi f\tau) d\tau \\
 &= \int_{-\infty}^{-2n\tau_d} \exp \left(- \frac{4n\tau_d}{\tau_c} \right) \exp(-j2\pi f\tau) d\tau \\
 &\quad + \int_{-2n\tau_d}^0 \exp \left(\frac{2\tau}{\tau_c} \right) \exp(-j2\pi f\tau) d\tau \\
 &\quad + \int_0^{2n\tau_d} \exp \left(- \frac{2\tau}{\tau_c} \right) \exp(-j2\pi f\tau) d\tau \\
 &\quad + \int_{2n\tau_d}^{+\infty} \exp \left(- \frac{4n\tau_d}{\tau_c} \right) \exp(-j2\pi f\tau) d\tau \\
 &= \exp \left(- \frac{4n\tau_d}{\tau_c} \right) \left[\int_{-\infty}^{+\infty} \exp(-j2\pi f\tau) d\tau \right. \\
 &\quad \left. - \int_{-2n\tau_d}^{+2n\tau_d} \exp(-j2\pi f\tau) d\tau \right] \\
 &\quad + \int_{-2n\tau_d}^0 \exp \left[\left(\frac{2}{\tau_c} - j2\pi f \right) \tau \right] d\tau \\
 &\quad + \int_0^{2n\tau_d} \exp \left[\left(- \frac{2}{\tau_c} - j2\pi f \right) \tau \right] d\tau \\
 &= \exp \left(- \frac{4n\tau_d}{\tau_c} \right) \left[\delta(f) - \frac{\sin(4n\pi\tau_d f)}{\pi f} \right] + \frac{\tau_c}{1 + (\pi f\tau_c)^2} \\
 &\quad \times \left\{ 1 - \exp \left[- \frac{4n\tau_d}{\tau_c} \right] \right. \\
 &\quad \left. \times [\cos(4n\pi f\tau_d) - \pi f\tau_c \sin(4n\pi f\tau_d)] \right\}. \tag{55}
 \end{aligned}$$

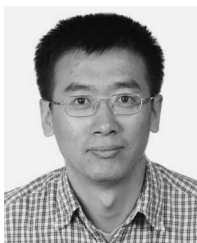
ACKNOWLEDGMENT

The authors would like to thank J. Oldham and D. Barlow of the Communications Research Centre, Canada, and F. Zeng and X.-F. Chen of the University of Ottawa, Ottawa, ON, Canada, for their assistance in setting up the experimental system.

REFERENCES

- [1] B. Mukherjee, "WDM optical communication networks: Progress and challenges," *IEEE J. Sel. Areas Commun.*, vol. 18, no. 10, pp. 1810–1824, Oct. 2000.
- [2] A. J. Cooper, "Fibre/radio for the provision of cordless/mobile telephony services in the access network," *Electron. Lett.*, vol. 26, no. 24, pp. 2054–2056, Nov. 1990.
- [3] H. Ogawa, D. Polifko, and S. Banba, "Millimeter-wave fiber optics systems for personal radio communication," *IEEE Trans. Microw. Theory Tech.*, vol. 40, no. 12, pp. 2285–2293, Dec. 1992.
- [4] A. J. Seeds, "Broadband wireless access using millimetre-wave over fibre systems," in *Proc. IEEE MTT-S Int. Microw. Symp.*, 1997, pp. 23–25. TU1B-1.
- [5] D. Novak, "The merging of the wireless and fiberoptic worlds," in *CLEO Tech. Dig.*, 2002, p. 276. Paper CTuS1.
- [6] L. Nöel, D. Wake, D. G. Moodie, D. D. Marcenac, L. D. Westbrook, and D. Nasset, "Novel techniques for high capacity 60 GHz fiber-radio transmission systems," *IEEE Trans. Microw. Theory Tech.*, vol. 45, no. 8, pp. 1416–1423, Aug. 1997.
- [7] M. Golubkoff, E. Pénard, D. Tanguy, P. Legaud, D. Mathoorasing, F. Devaux, and C. Minot, "Outdoor and indoor applications for broadband local loop with fibre supported millimeter-wave radio systems," in *IEEE MTT-S Int. Microw. Symp. Tech. Dig.*, 1997, pp. 31–34. Paper TU1B-3.
- [8] J. E. Román, L. T. Nichols, K. J. Williams, R. D. Esman, G. C. Tavik, M. Livingston, and M. G. Parent, "Fiber-optic remoting of an ultrahigh dynamic range radar," *IEEE Trans. Microw. Theory Tech.*, vol. 46, no. 12, pp. 2317–2323, Dec. 1998.
- [9] E. C. Niehenke and P. Hercafeld, "An optical link for W-band transmit/receive applications," in *Proc. IEEE MTT-S Int. Microw. Symp. Tech. Dig.*, 1997, pp. 35–38. Paper TU1B-4.
- [10] J. L. Corral, J. Marti, J. M. Fuster, R. Laming, and M. J. Cole, "Continuously variable true time-delay optical feeder for phased-array antenna employing chirped fiber gratings," *IEEE Trans. Microw. Theory Tech.*, vol. 45, no. 8, pp. 1531–1536, Aug. 1997.
- [11] R. P. Braun, G. Grosskopf, D. Rohde, and F. Schmidt, "Optical millimetre-wave generation and transmission experiments for mobile 60 GHz band communications," *Electron. Lett.*, vol. 32, no. 7, pp. 626–628, Mar. 1996.
- [12] L. Goldberg, H. F. Taylor, J. F. Weller, and D. M. Bloom, "Microwave signal generation with injection-locked laser diodes," *Electron. Lett.*, vol. 19, no. 13, pp. 491–493, 1983.
- [13] R. T. Ramos and A. J. Seeds, "Fast heterodyne optical phase lock loop using double quantum well laser diodes," *Electron. Lett.*, vol. 28, no. 1, pp. 82–83, Jan. 1992.
- [14] L. N. Langley, M. D. Elkin, C. Edge, M. J. Wale, U. Gliese, X. Huang, and A. J. Seeds, "Packaged semiconductor laser optical phase-locked loop (OPLL) for photonic generation, processing and transmission of microwave signals," *IEEE Trans. Microw. Theory Tech.*, vol. 47, no. 7, pp. 1257–1264, Jul. 1999.
- [15] J. J. O'Reilly, P. M. Lane, R. Heidemann, and R. Hofstetter, "Optical generation of very narrow linewidth millimetre wave signals," *Electron. Lett.*, vol. 28, no. 25, pp. 2309–2311, Dec. 1992.
- [16] J. J. O'Reilly and P. M. Lane, "Fibre-supported optical generation and delivery of 60 GHz signals," *Electron. Lett.*, vol. 30, no. 16, pp. 1329–1330, Aug. 1994.
- [17] P. Shen, N. J. Gomes, P. A. Davies, W. P. Shillue, P. G. Huggard, and B. N. Ellison, "High-purity millimetre-wave photonic local oscillator generation and delivery," in *Proc. Microw. Photon.*, 2003, pp. 189–192.
- [18] P. O. Hedekvist, B. E. Olsson, and A. Wiberg, "Harmonic generation of photonic microwave frequencies utilizing the properties of a phase modulator," in *Proc. Microw. Photon.*, 2003, pp. 193–196.
- [19] X. J. Meng and J. Menders, "Optical generation of microwave signals using SSB-based frequency-doubling scheme," *Electron. Lett.*, vol. 39, no. 1, pp. 103–105, Jan. 2003.
- [20] G. Qi, J. Yao, J. Seregelyi, S. Paquet, and J. C. Bélisle, "Millimeter-wave carrier generation using an optical phase modulator and an optical notch filter," presented at Photonics North, vol. SPIE-5579C, Ottawa, ON, Canada, 2004, Paper 102.

- [21] F. N. Timofeev, S. Bennett, R. Griffin, P. Bayvel, A. J. Seeds, R. Wyatt, R. Kashyap, and M. Robertson, "High spectral purity millimetre-wave modulated optical signal generation using fibre grating lasers," *Electron. Lett.*, vol. 34, no. 7, pp. 668–669, Apr. 1998.
- [22] J. J. O'Reilly and M. Lane, "Remote delivery of video services using millimeter-wave and optics," *J. Lightw. Technol.*, vol. 12, no. 2, pp. 369–375, Feb. 1994.
- [23] W. Shieh and L. Maleki, "Phase noise of optical interference in photonic RF systems," *IEEE Photon. Tech. Lett.*, vol. 10, no. 11, pp. 1617–1619, Nov. 1998.
- [24] P. J. Matthews and R. D. Esman, "Intrinsic microwave phase noise of fiber-optic links," in *IEEE MTT-S Int. Microw. Symp. Tech. Dig.*, 1998, pp. 1517–1519. Paper TH3C-3.
- [25] M. Bibey, F. Deborgies, M. Krakowski, and D. Mongardien, "Very low phase-noise optical links-experiments and theory," *IEEE Trans. Microw. Theory Tech.*, vol. 47, no. 12, pp. 2257–2261, Dec. 1999.
- [26] R. Hofstetter, H. Schmuck, and R. Heidemann, "Dispersion effects in optical millimeter-wave systems using self-heterodyne method for transport and generation," *IEEE Trans. Microw. Theory Tech.*, vol. 43, no. 9, pp. 2263–2269, Sep. 1995.
- [27] U. Gliese, S. Norskov, and T. N. Nielsen, "Chromatic dispersion in fiber-optic microwave and millimeter-wave links," *IEEE Trans. Microw. Theory Tech.*, vol. 44, no. 10, pp. 1716–1724, Oct. 1996.
- [28] B. Pourbahri, P. A. Davies, D. S. George, and D. Wake, "The effects of fiber amplifier phase noise on radio over fibre signals," in *Proc. Broadband Commun.*, Feb. 2000, pp. 89–91.
- [29] G. J. Cowle, P. R. Morkel, R. I. Laming, and D. N. Payne, "Spectral broadening due to fibre amplifier phase noise," *Electron. Lett.*, vol. 26, no. 7, pp. 424–425, Mar. 1990.
- [30] J. Rogers and C. Plett, *Radio Frequency Integrated Circuit Design*. Norwood, MA: Artech House, 2003, pp. 283–287.
- [31] A. G. Armada and M. Calvo, "Phase noise and sub-carrier spacing effects on the performance of an OFDM communication system," *IEEE Commun. Lett.*, vol. 2, no. 1, pp. 11–13, Jan. 1998.
- [32] K. Okamoto, *Fundamentals of Optical Waveguides*. New York: Academic, 2000, pp. 159–161.
- [33] J. Rutman and F. L. Walls, "Characterization of frequency stability in precision frequency sources," *Proc. IEEE*, vol. 79, no. 7, pp. 952–960, Jul. 1991.
- [34] A. Papoulis, *Probability, Random Variables, and Stochastic Processes*. New York: McGraw-Hill, 1984.
- [35] H. E. Rowe, *Signals and Noise in Communication Systems*. New York: Van Nostrand, 1965. P130.
- [36] Product Note 11729B-1, *Phase Noise Characterization of Microwave Oscillators-Phase Detector Method*, Palo Alto, CA: Hewlett Packard.
- [37] W. P. Robins, *Phase Noise in Signal Sources*. London, U.K.: Peter Peregrinus, 1982, pp. 77–78.
- [38] G. Qi, J. P. Yao, J. Seregelyi, C. Bélisle, and S. Paquet, "Optical generation and distribution of continuously tunable millimeter-wave signals using an optical phase modulator," *J. Lightw. Technol.*, vol. 23, no. 9, pp. 2687–2695, Sep. 2005.
- [39] E. Costa and S. Pupolin, "M-QAM-OFDM system performance in the presence of a nonlinear amplifier and phase noise," *IEEE Trans. Commun.*, vol. 50, no. 3, pp. 462–472, Mar. 2002.
- [40] J. W. Goodman, *Statistical Optics*. New York: Wiley, 1985, pp. 167–168.
- [41] L. E. Richter, H. I. Mandelberg, M. S. Kruger, and P. A. McGrath, "Linewidth determination from self-heterodyne measurements with sub-coherence delay times," *IEEE J. Quantum Electron.*, vol. QE-22, no. 11, pp. 2070–2074, Nov. 1986.



Guohua Qi received the B.E. and M.S. degrees in electrical engineering from Beijing University of Posts and Telecommunications, Beijing, China, in 1986 and 1989, respectively. He is currently working toward the Ph.D. degree in information technology and engineering at the University of Ottawa, Ottawa, ON, Canada.

In 1989, he joined the Nanjing Electronic Devices Institute (NEDI), Nanjing, China, where he was engaged in the research and development of microwave solid-state circuits, modules, and subsystems for

12 years. He joined Wi-Sys Communications Inc., Ottawa, in 2005. His current research interests include microwave photonics, radio over fiber, RF and microwave circuits, and software-defined radio.



Jianping Yao (M'99–SM'01) received the Ph.D. degree in electrical engineering from Université de Toulon, Toulon, France, in 1997.

From 1999 to 2001, he held a faculty position with the School of Electrical and Electronic Engineering, Nanyang Technological University, Singapore. In 2001, he joined the School of Information Technology and Engineering, University of Ottawa, ON, Canada, where he is a Professor and Director of the Microwave Photonics Research Laboratory. He was a Guest Professor with Shantou University and Sichuan University, China, and was an Invited Professor with the Institut National Polytechnique de Grenoble, France, in 2005. His research has focused on microwave photonics, which includes all-optical microwave signal processing, photonic generation of microwave, millimeter wave and terahertz, radio over fiber, UWB over fiber, FBGs for microwave photonics applications, and optically controlled phased array antennas. His research interests also include fiber lasers, fiber-optic sensors, and biophotonics. He has published over 130 papers in refereed journals and conference proceedings.

Dr. Yao is a member of SPIE, OSA, and a Senior Member of IEEE/LEOS and IEEE/MTT.



Joe Seregelyi received the M.Eng. degree in engineering physics from McMaster University, Hamilton, ON, Canada, in 1987.

In 1988, he joined the National Research Council, where he was involved in the area of pulsed electromagnetics. Since 1993, he has been with the Communications Research Centre, Ottawa, ON, where he is currently the Research Engineering/Project Leader of microwave photonics. He has authored or coauthored over 50 technical papers and reports. He holds patents in the area of hybrid infrared (IR)/high-power microwaves (HPM) landmine detection and neutralization. He possesses extensive knowledge in the areas of RF and microwave design (signal integrity, circuit design, electromagnetic compatibility, antenna design, HPMS, and ultrawideband radar and communications). He has also been involved with optical design for a number of years (high-power lasers, antenna remoting, communications systems, and IR imaging).



Stéphane Paquet received the M.Sc. degree in optics from Laval University, Quebec City, QC, Canada, in 1993.

He then joined the National Optics Institute, where he was involved with the design and fabrication of integrated optics components. He then joined MPB Technologies, Montreal, QC, as a member of the Space Technology Group and Optical Amplifier Research and Development Group. In 1997, he joined Nortel Networks, Montreal, where he was initially a member of the Communication Systems Engineering Group. He was then an Optical System Designer with Nortel Networks, Ottawa, ON, Canada, and a Researcher with the Optical Components Research and Development Group, Nortel Networks, Harlow, U.K. He is currently with the Communications Research Centre, Ottawa, where he is involved in the microwave photonic research field.



Claude Bélisle received the Bachelors degree in engineering physics from the Royal Military College of Canada, Kingston, ON, Canada, and the Masters degree in physics-optics from Laval University, Quebec City, QC, Canada.

He has been involved in various research and development projects related to satellite communications for both military and commercial applications with the DRDC–Ottawa and Communications Research Centre, Ottawa, ON. He is currently the Research Manager with the CRC Advanced Radio System Group, where he leads research in microwave-photonics technologies, satellite communications networks, and SDR. He is also a Director with the Software Defined Radio Forum.



Xiupu Zhang (M'00) received the M.Sc. degree from Beijing University of Posts and Telecommunications, Beijing, China, and the Ph.D. degree from Technical University of Denmark, Lyngby, Denmark, in 1988 and 1996, respectively, both in electrical engineering.

Following his Ph.D. study, he became a Research Fellow with Chalmers University of Technology, Gothenburg, Sweden, for one and a half years. Prior to joining Concordia University, Montréal, QC, Canada, in June 2002, he had worked in the fiber-

optics industry in China, Canada, and the United States for about ten years. Currently, he is an Associate Professor with the Department of Electrical and Computer Engineering, Concordia University. His current research interests include optical fiber transmission, radio-over-fiber systems, passive optical networks, and broadband optical sources.

Dr. Zhang is a member of OSA.



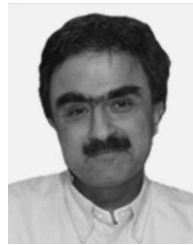
Ke Wu (M'87–SM'92–F'01) received the B.Sc. degree (with distinction) in radio engineering from Nanjing Institute of Technology (now Southeast University), Nanjing, China, in 1982, the D.E.A. degree from the Institut National Polytechnique de Grenoble, Grenoble, France, in 1984, and the Ph.D. degree (with distinction) from the University of Grenoble, Grenoble, in 1987, both in optics, optoelectronics, and microwave engineering.

He is a Professor of electrical engineering and the Tier-I Canada Research Chair in RF and millimeter-

wave engineering with the Ecole Polytechnique-University of Montreal, Montreal, QC, Canada. He was a Visiting or Guest Professor with many universities and research institutions. He also holds an honorary visiting professorship and a Cheung-Kong-endowed chair professorship (visiting) at the Southeast University, and an honorary professorship at the Nanjing University of Science and Technology, Nanjing, and the City University of Hong Kong, Kowloon, Hong Kong. He has also been the Director of the Poly-Grames Research Center. He has authored or coauthored more than 500 referred papers and several books/book chapters. He serves on the Editorial Board of the *Microwave Journal*, *Microwave and Optical Technology Letters* and Wiley's *Encyclopedia of RF and Microwave Engineering*. He is an Associate Editor of the *International Journal of RF and Microwave Computer-Aided Engineering*. His current research interests include substrate integrated circuits, antenna arrays, advanced CAD and modeling techniques, development of low-cost RF and millimeter-wave transceivers, and modeling and design of microwave photonic circuits and systems.

Dr. Wu is a member of the Electromagnetics Academy, the Sigma Xi Honorary Society, and the URSI, and a Fellow of the Canadian Academy of Engineering and the Royal Society of Canada (The Canadian Academy of the Sciences and Humanities). He has held many positions in and has served on various international committees, including the Vice-Chairperson of the Technical Program Committee (TPC) for the 1997 Asia-Pacific Microwave Conference (APMC), the General Co-Chair of the 1999 and 2000 SPIE's International Symposium on Terahertz and Gigahertz Electronics and Photonics, the General Chair of the 8th International Microwave and Optical Technology

(ISMOT'2001), the TPC Chair of the 2003 IEEE Radio and Wireless Conference (RAWCON'2003), the General Co-Chair of the RAWCON'2004, and the Co-Chair of the 2005 APMC International Steering Committee. He will be the General Chair of the 2012 IEEE MTT-S International Microwave Symposium (IMS) and the 2007 URSI International Symposium on Signals, Systems and Electronics (ISSSE). He served on the 1996 IEEE Admission and Advancement Committee, the Steering Committee for the 1997 joint IEEE Antennas and Propagation Society/URSI International Symposium, and the TPC for the IEEE MTT-S International Microwave Symposium. He was elected into the Board of Directors of the Canadian Institute for Telecommunication Research. He is currently the Chair of the joint IEEE chapters of MTT/APS/LEOS in Montreal. He is an elected MTT-S AdCom Member for 2006-2009 and serves as the Chair of the IEEE MTT-S Transnational Committee. He has served on the Editorial or Review Boards of various technical journals, including the IEEE TRANSACTIONS ON MICROWAVE THEORY AND TECHNIQUES, the IEEE TRANSACTIONS ON ANTENNAS AND PROPAGATION, and the IEEE MICROWAVE AND WIRELESS COMPONENTS LETTERS. He was a recipient of the URSI Young Scientist Award, the Oliver Lodge Premium Award of the Institute of Electrical Engineers, U.K., the Asia-Pacific Microwave Prize, the IEEE CCECE Best Paper Award, the University Research Award "Prix Poly 1873 pour l'Excellence en Recherche" presented by the Ecole Polytechnique on the occasion of its 125th anniversary, the Urgel-Archambault Prize (the highest honor) in the field of physical sciences, mathematics, and engineering from the French-Canadian Association for the Advancement of Science, and the 2004 Fessenden Medal of the IEEE Canada. In 2002, he was the first recipient of the IEEE MTT-S Outstanding Young Engineer Award.



Raman Kashyap received the B.Sc. degree from King's College, London, U.K., and the Ph.D. degree in physics from Essex University, Colchester, U.K.

He is currently a Professor jointly with the Departments of Electrical Engineering and Physics Engineering, École Polytechnique de Montréal, Montréal, QC, Canada. He is the Head with the Advanced Photonics Concepts Laboratory. He has been active in the field of photonics research for 30 years, many of which were spent at British Telecom Research Laboratories at Martlesham Heath, Ipswich, U.K.

He has worked on optical fiber-based devices, measurements, and nonlinear optics. He researched fiber Bragg gratings since the very early day of the field and published more than 250 papers in journals, books, and conferences. He has presented numerous invited talks at conferences and institutes around the world, authored the first book on fiber Bragg gratings, and has filed over 35 patents. His current research interest centers around advanced application in photonics, including signal processing, glass and waveguide poling, advanced Bragg gratings, single frequency sources, radio over fiber, negative refractive index devices, photonic crystal structures, biophotonics, nonlinear optics, and integrated optic waveguides.

Prof. Kashyap is a Chartered Physicist, a fellow of the Optical Society of America, and a member of the IEE. He currently holds the Canada Research Chair on Future Photonic Systems. He is the Chair of the subcommittee of Guided-Wave Devices of Photonics North 2007 and on the International Program Committee of the International Conference on Optical and Optoelectronic Properties of Materials and Applications (ICOOPMA), for 2006 and 2007.